Volume 16
Number 42
14 November 2020
Pages 9605–9824

Soft Matter

rsc.li/soft-matter-journal

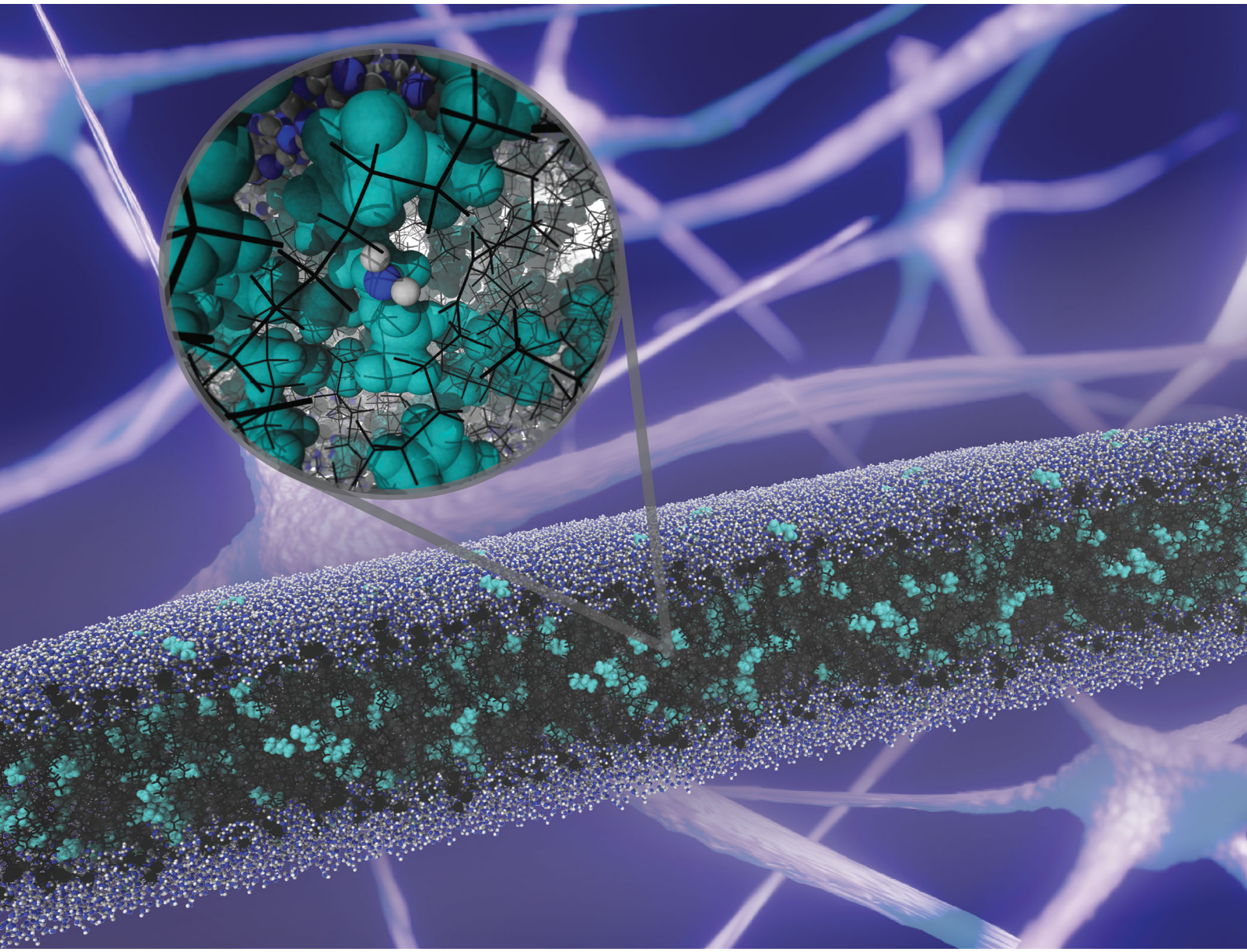

ISSN 1744-6848

ROYAL SOCIETY OF CHEMISTRY

PAPER
Maikel C. Rheinstädter *et al.*
Anesthetics significantly increase the amount of intramembrane water in lipid membranes

Soft Matter

PAPER

View Article Online
View Journal | View Issue

Cite this: *Soft Matter*, 2020, **16**, 9674

Anesthetics significantly increase the amount of intramembrane water in lipid membranes†

Sebastian Himbert,[a] Lili Zhang,[a] Richard J. Alsop,[a] Viviana Cristiglio,[b] Giovanna Fragneto[b] and Maikel C. Rheinstädter*[a]

Received 10th July 2020,
Accepted 21st August 2020

DOI: 10.1039/d0sm01271h

rsc.li/soft-matter-journal

The potency of anesthesia was directly linked to the partitioning of the drug molecules in cell membranes by Meyer and Overton. Many molecules interact with lipid bilayers and lead to structural and functional changes. It remains an open question which change in membrane properties is responsible for a potential anesthetic effect or if anesthetics act by binding to direct targets. We studied the effect of ethanol, diethyl ether and isoflurane on the water distribution in lipid bilayers by combining all-atom molecular dynamics simulations and neutron diffraction experiments. The simulations show strong membrane–drug interactions with partitioning coefficients of 38%, 92% and 100% for ethanol, diethyl ether and isoflurane, respectively, and provide evidence for an increased water partitioning in the membrane core. The amount of intramembrane water molecules was experimentally determined by selectively deuterium labeling lipids, anesthetic drug and water molecules in neutron diffraction experiments. Four additional water molecules per lipid were observed in the presence of ethanol. Diethyl ether and isoflurane were found to significantly increase the amount of intramembrane water by 25% (8 water molecules). This increase in intramembrane water may contribute to the non-specific interactions between anesthetics and lipid membranes.

1 Introduction

The first reported use of anesthesia in surgery dates back more than 150 years ago when diethyl ether was used during a tooth extraction. Rather than being the result of careful studies and extended research, the idea to this novel approach for pain relief was a byproduct of so called 'ether parties', popular among medical and chemistry students.[2] Nowadays, numerous anesthetic drugs are known and used every day in hospitals around the world. However, our knowledge of the molecular mode of action of these drugs is surprisingly limited. It is an ongoing debate whether anesthetics act by binding to direct targets, or act through non-specific interactions with the lipid bilayer.[3]

While the $GABA_A$ receptor has been identified as target for propofol and ethomidate,[4] the situation is less clear for other commonly known anesthetics.[3] Based on the Meyer–Overton correlation, anesthetic potency was found to be directly related to their lipid solubility.[5–7] This correlation suggests an indirect mechanism where the activity of membrane proteins is modulated by variations in membrane properties in the presence of anesthetic molecules. Membrane characteristics, such as hydrophobic thickness, dipole potential, fluidity, curvature, elastic properties, proximity to phase transitions, and the degree of lateral microheterogeneity, all vary with membrane composition and have been shown to have a strong influence on membrane protein function.[3,8,9] A wide variety of molecules interact with lipid bilayers leading to structural and functional changes. However, it remains an open question how the interactions of anesthetic drugs differ from other molecules.

As first demonstrated by Ashcroft *et al.*, benzyl alcohol incorporates in the head group region of lipid bilayers leading to an increased membrane thickness.[1] It was proposed that this increased head-to-head distance is the result of induced order of the lipid molecules leading to a radial compressive stress onto embedded sodium channels, as depicted in Fig. 1. By using a combination of neutron scattering and Molecular Dynamics (MD) simulations, it was demonstrated in the case of the anesthetic drug Ketamine, that physiological quantities can alter the lateral membrane pressure and may affect the function of embedded membrane channels.[3] However, studies of different anesthetic molecules did not show a similar increase in membrane thickness.[10]

While the effect of anesthetics on a number of membrane properties has been studied, little attention has been given to

[a] *Department of Physics and Astronomy, McMaster University, ABB-241, 1280 Main Street West, Hamilton, Ontario L8S 4M1, Canada. E-mail: rheinstadter@mcmaster.ca; Fax: +1-905-546-1252; Tel: +1-905-525-9140-23134*

[b] *Institut Laue-Langevin, B.P. 156, 38042 Grenoble Cedex, France*

† Electronic supplementary information (ESI) available. See DOI: 10.1039/d0sm01271h

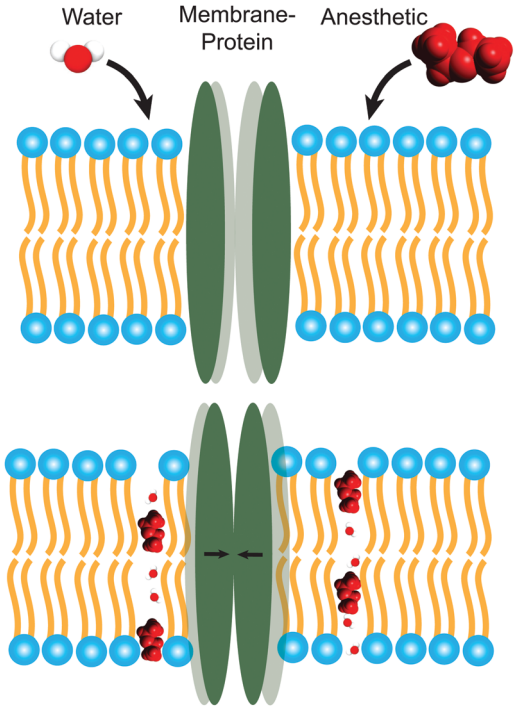

Fig. 1 First proposed by Ashcroft *et al.*,[1] it is widely accepted that anesthetic molecules incorporate into lipid bilayers. By changing membrane properties, such as hydrophobic thickness, dipole potential, fluidity, curvature elastic properties, and lateral membrane pressure, anesthetics can change protein conformations and activity.

potential changes in the amount and distribution of intramembrane water molecules. In fact, little is known about the effect of anesthetic drugs on the membrane's water permeability, likely due to the challenges related to a precise measurement of water inside of bilayers. While previous studies reported a decrease in membrane permeability in a 1 molar ethanol solution,[11,12] Toppozini *et al.*[13] tentatively assigned 2 additional water molecules per lipid in the hydrophobic membrane core when the membranes were immersed in a 5 mol% ethanol solution. However, they could not uniquely distinguish between ethanol and water molecules from their X-ray diffraction data.

It is experimentally challenging to probe the water distribution across a lipid bilayer on a molecular scale. While techniques such as X-ray diffraction provide high-resolution structural data on a membrane assembly, they fail to contrast water from lipid and anesthetic molecules just based on their number of electrons. Neutrons, on the other hand, interact with the atomic nuclei of atoms and are highly sensitive to isotopical composition. While being indistinguishable for X-ray scattering, deuterium (H^2) has a coherent neutron scattering cross section that is $\sim$3 times higher than hydrogen (H^1). Hydrating solid supported membranes with D_2O thus allows to contrast water molecules against protonated membranes and anesthetic molecules.

In this study we investigate the effect of ethanol, diethyl ether and isoflurane on the intramembrane water distribution in a lipid bilayer using a combination of MD simulations and neutron diffraction. Water molecules within the bilayers were made visible in the experiments through selective deuterium labeling and we found that anesthetics can lead to a significant increase of intramembrane water.

2 Results

2.1 Molecular dynamics simulations

MD simulations of a POPC patch containing 128 POPC molecules including 35 water molecules per lipid and 200 molecules of the respective anesthetic drug were performed. The skeletal formula of ethanol, diethyl ether and isoflurane are depicted in Fig. 2(a). Snapshots of the simulations after 200 ns are shown in Fig. 2(b–e). Ethanol, diethyl ether and isoflurane are depicted in green, purple and cyan respectively. Water molecules are represented by white and red spheres symbolizing oxygen and hydrogen. The lipid tails are omitted for clarity and only the phosphate atom of POPC is visualized as blue sphere. While the diethyl ether and isoflurane molecules are located inside the bilayer, the ethanol molecules are mainly found in the head group region of the membrane. Partitioning for diethyl ether and isoflurane appears to be almost complete while the adsorbed ethanol molecules are in equilibrium with molecules dissolved in the hydration water layer.

The partitioning coefficient, *i.e.* the fraction of inserted molecules as function of simulation time is shown in Fig. 3(a). Partitioning coefficients of 98 $\pm$ 1% and 93 $\pm$ 2% were determined for isoflurane and diethyl ether, respectively. In the case of ethanol, 38 $\pm$ 4% of the molecules interacted with the membrane. While isoflurane and ethanol molecules partitioned within the first 20 ns of the simulations, the final value for diethyl ether was observed after 200 ns, only.

Scattering length density (SLD) profiles were calculated for all systems and are graphed in Fig. 3(b). The simulated SLDs for POPC, ethanol, diethyl ether, isoflurane and D_2O are shown as dotted lines. The scattering contributions of ethanol and diethyl ether are small and the molecules do not contribute significantly to the total SLD. Isoflurane led to a significantly increased SLD in the membrane core as a result of the high scattering length (5.654 fm[14]) of the fluorine atoms. The SLD reaches 5.6×10^{-6} 1 $Å^{-2}$ in the water layer for a pure POPC bilayer and systems containing diethyl ether and isoflurane. The SLD is significantly reduced in the water layer in the presence of ethanol to a value of 5.3×10^{-6} 1 $Å^{-2}$ due to ethanol's low partitioning coefficient and the presence of dissolved ethanol molecules. While the ethanol sample shows a slight increase of the SLD in the head group region, the SLD profile of the diethyl ether sample is unchanged as compared to the pure POPC patch. The integrated SLDs, *i.e.* the total scattering contribution, for the different components are listed in Table 1.

We note that it is not easily possible to study transmembrane water transport if it is not facilitated by, for instance, a water channel such as aquaporine, within typical simulation times of hundreds of nanoseconds. Spontaneous events, in

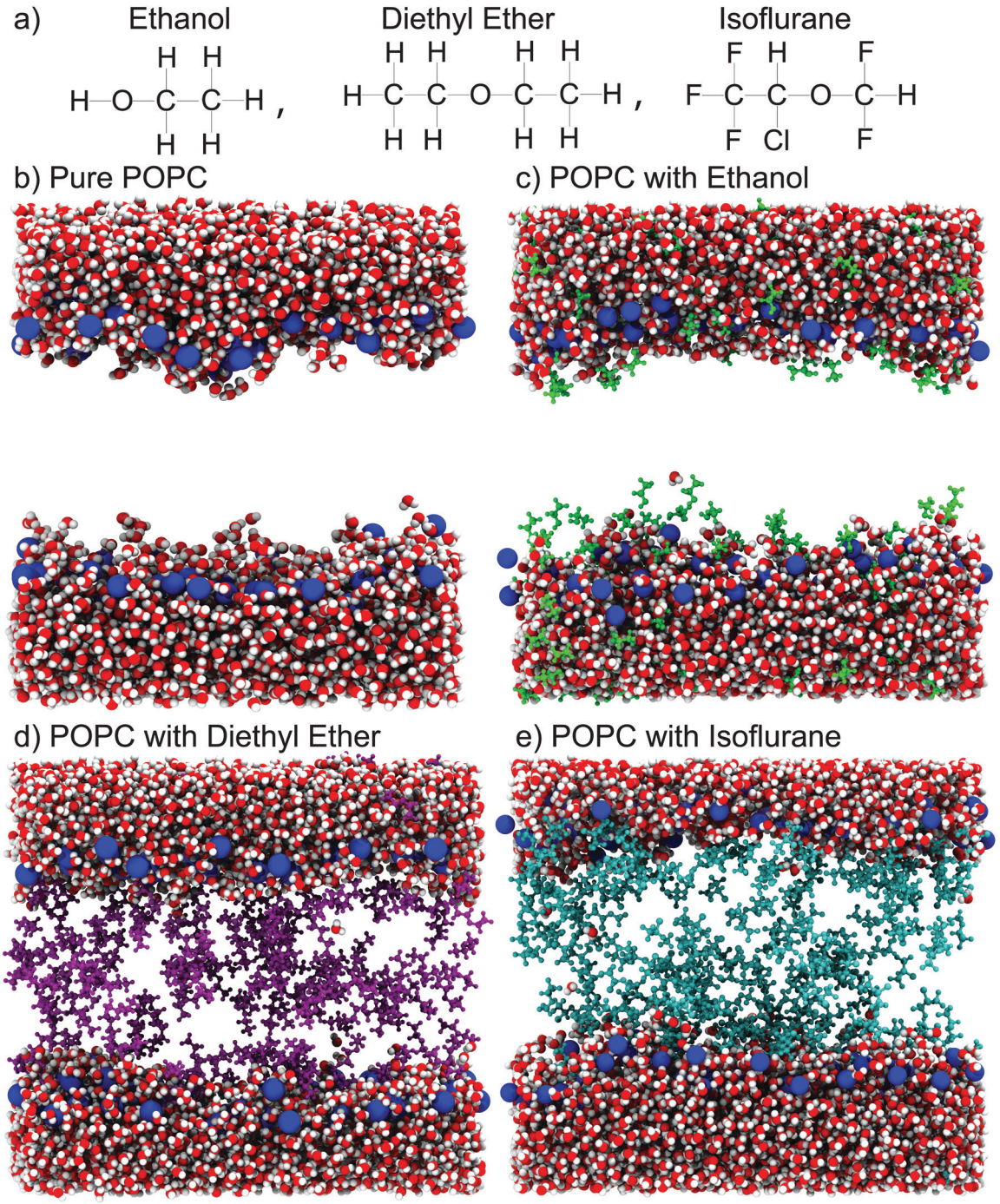

Fig. 2 (a) Skeletal formula of ethanol, diethyl ether and isoflurane. (b–e) Snapshots of the MD simulations after 200 ns of simulation. The lipid tails are omitted for clarity. A pure POPC bilayers is shown in (a). Ethanol (b) preferably partitioned in the head group region of the bilayers and the simulations show an equilibrium between adsorbed ethanol molecules and molecules in solution. Diethyl ether in (c) and isoflurane (d) were found to spontaneously partition in the membrane core.

comparison, are rare,[15–17] and the number of intramembrane water molecules depends on system size and duration of the simulations. While some water molecules can indeed be seen in the MD snapshots in Fig. 2(b–e) (and in the MD videos in the ESI,† S1–S4), the time-averaged intramembrane water concentration is too small to significantly contribute to the membranes' SLDs. The MD simulation profiles were used to determine the contributions of POPC, ethanol, diethyl ether and isoflurane to the experimental SLD, as shown below.

Umbrella simulations were conducted to determine the potential mean force (PMF) profile $W(z)$ of water molecules, as shown in Fig. 4(a). The pure POPC bilayer shows a high energy barrier of up to $\sim$26 kJ mol^{-1} in the membrane core, in good agreement with previously published results.[18] The addition of

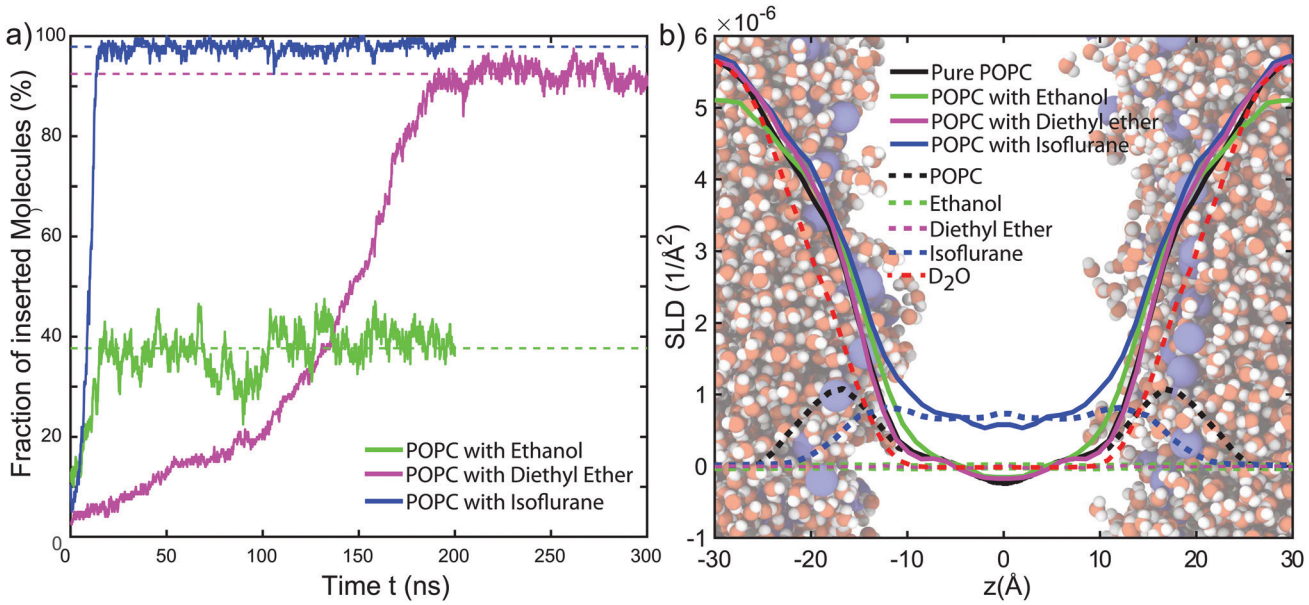

Fig. 3 (a) Fraction of inserted anesthetic molecules as function of simulation time. While only 38% of ethanol molecules partitioned in the lipid bilayers, 93% of diethyl ether and 98% of isoflurane molecules located inside the membranes. (b) Scattering length density (SLD) profiles for POPC, POPC/ethanol, POPC/diethyl ether and POPC/isoflurane. The individual contributions of ethanol, dethyl ether, isoflurane, and D_20 are shown as dotted lines.

Table 1 Integrated scattering length densities determined from MD Simulations

System	Integrated SLD ($Å^{-1}$)
POPC	1.9×10^{-5}
POPC head group	7.9×10^{-6}
POPC tails	1.2×10^{-5}
Ethanol	-4.4×10^{-7}
Diethyl ether	-4.1×10^{-7}
Isoflurane	2.6×10^{-5}

ethanol led to a slight decrease in the barrier width while diethyl ether significantly lowered the energy barrier. Isoflurane was found to show a negative potential mean force.

The diffusion coefficient of the hydration water molecules was calculated from their auto correlation function (as detailed in Materials and methods) and is shown in Fig. 4(b). The profiles reach values of $D \approx 4$ cm^2 s^{-1} at $|z| > 25$ Å. In the case of a pure POPC bilayer, the diffusion constant is increased in the bilayer center, between both leaflets. This central peak can no longer be observed in the presence of anesthetic molecules. In addition, the molecules led to an increase in diffusivity in the head group region. The combination of the PMF $W(z)$ and the Diffusivity $D(z)$ allows calculating the water partitioning coefficient, K, and water permeability P of the bilayers, as described in the Materials and methods Section. The relative change in the permeability, K/K_{POPC}, and the relative partitioning coefficient, P/P_{POPC}, are shown in Fig. 4(c and d). The presence of anesthetic molecules was found to significantly increase both measures. While the partitioning coefficient K was unchanged in the presence of ethanol (within the errors), it increased by factors of 2 and 60 in case of diethyl ether and isoflurane, respectively. Similarly, the permeability increased by a factor of 1000 (diethyl ether) and 10 000 (isoflurane), while ethanol did not alter the permeability. The area per lipid in the presence of the different compounds was determined to be: 62.84 Å^2 (POPC), 67.75 Å^2 (POPC/ethanol), 77.90 Å^2 (POPC/diethyl ether), and 77.60 Å^2 (POPC/isoflurane).

2.2 Neutron diffraction experiment

The water concentration along the bilayer normal was experimentally determined using neutron diffraction. All experiments were performed on the D16 neutron diffractometer[19] at the Institut Laue-Langevin (ILL) in Grenoble, France. The setup is sketched in Fig. 5(a). Reflectivity (along the q_z-axis) was measured up to $q_z = 0.9$ Å^{-1} using D16's 2-dimensional detector, as shown in Fig. 5(b). Data were then integrated into line scans (Fig. 5(c)). Well pronounced specular Bragg peaks were observed in all samples indicating highly ordered membrane stacks. The lamellar d_z-spacings were determined from the peak positions to POPC: 53.1 ± 0.4 Å, POPC/ethanol: 53.1 ± 0.4 Å, POPC/diethyl ether: 52.3 ± 0.4 Å and POPC/isoflurane: 51.8 ± 0.4 Å.

The scattering contribution of water molecules was significantly enhanced in the experiments by selectively labeling the different components. Protonated lipids and anesthetic molecules were hydrated by heavy water (D_2O), whose coherent scattering contribution is dominating the signal. In contrast to the MD simulations, the experiment is mainly sensitive to the contributions from intramembrane water. Because of the corresponding large number of molecules and the long measurement times (in the order of several minutes per measurement point), large ensembles of molecules are probed over long periods of time as compared to molecular timescales, which are typically in the order of nanoseconds. While the

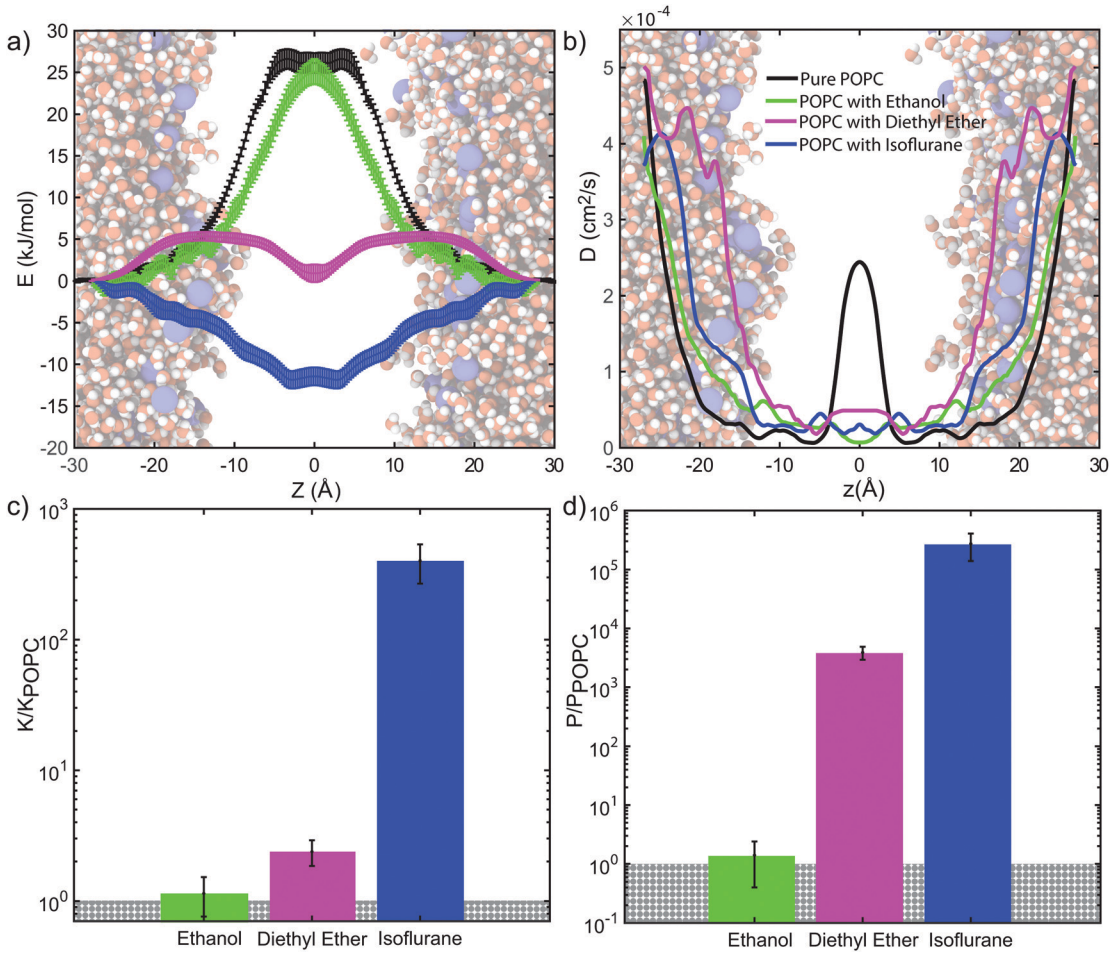

Fig. 4 (a) PMF $W(z)$ along the bilayer normal determined from umbrella sampling. While a pure POPC bilayer shows an energy barrier of up to $\approx$26 kJ mol^{-1}, the PMF is significantly reduced in the presence of anesthetic molecules. (b) The water diffusivity profile along the bilayer normal was determined from the ACF and eqn (1). The presence of anesthetic molecules resulted in a lowered diffusion constant in the bilayer center and an increased diffusivity around the lipid head groups. The water partitioning coefficient (c) defined by eqn (3), and water permeability (d), as determined by eqn (2), were significantly increased in the presence of anesthetic molecules. The values for POPC are indicated by the shaded area.

small number of molecules in the MD simulations and the relatively short simulation times resulted in a small probability of observing water molecules inside the membrane, their contribution is significant in the experiments.

The corresponding scattering length density (SLD) profiles were calculated by a 1-dimensional Fourier Analysis of the integrated peak intensities and are presented in Fig. 6(a). The SLD profiles are dominated by the contribution of D_2O. The high SLD at $|z| > 20$ Å indicates the water layer on either side of the bilayer. The SLD becomes significantly lower in the bilayer center indicating a water-poor region. While the presence of ethanol and diethyl ether showed little to no change, isoflurane resulted in a significantly increased SLD in the bilayer center. The SLD inside the hydrophobic core is small in the case of a pure POPC bilayer. Ethanol resulted in a slight increase in the SLD in the head group region, while diethyl ether showed an increased SLD towards the bilayer center. The number of water molecules in the unit cell was determined by integrating the experimental SLD and subtracting the contributions from POPC and the anesthetic molecules, which were determined in the MD simulations (see Materials and methods). From this combined analysis, the number of water molecules per lipid was determined, and is plotted in Fig. 6(b). 29.5 water molecules were observed for a pure POPC bilayer, 32 for ethanol, and up to 37.5 water molecules were observed in the presence of diethyl ether and isoflurane, respectively.

3 Discussion

By analyzing the experimental data in conjunction with results from the MD simulations we find evidence for 4 additional water molecules per lipid in the presence of ethanol, and 8 additional water molecules in the case of diethyl ether and isoflurane. While the integrated SLD only provides total numbers, it is not clear where these water molecules reside in the membranes. While the fluorine atoms of the isoflurane significantly contribute to the SLD, we consider the contribution of ethanol and diethyl ether to be negligible, as can be also seen in Table 1. Any deviation from the SLD of a pure POPC bilayer then

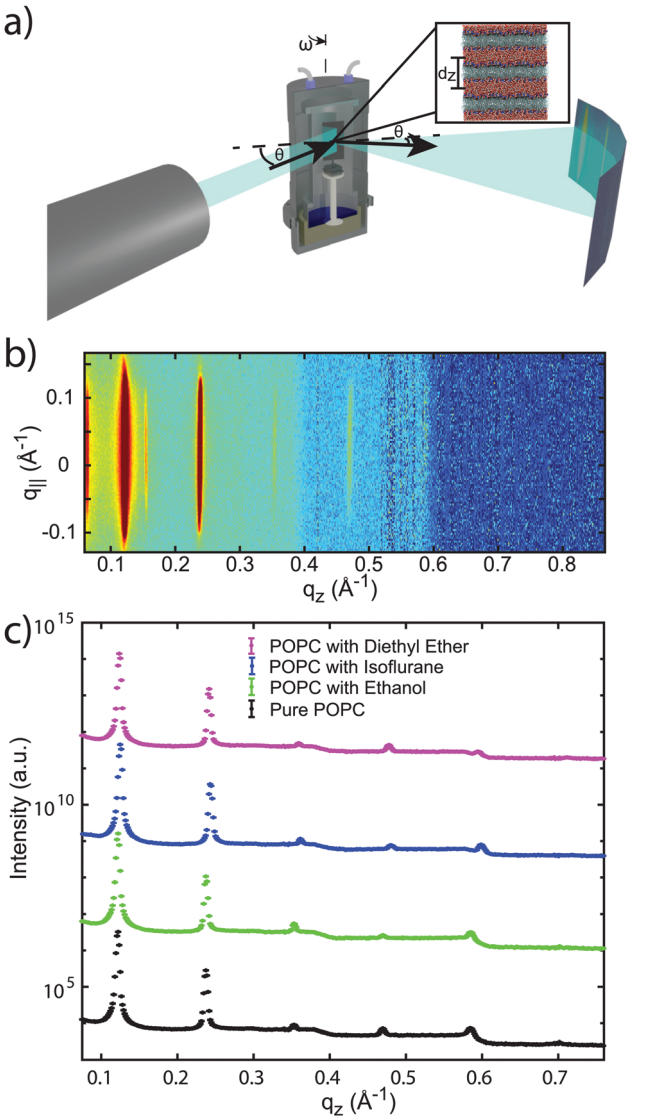

Fig. 5 (a) Schematic of the experimental setup. A silicon wafer carrying solid supported POPC membranes was mounted in a humidity and temperature controlled chamber. The container on the bottom of the chamber was filled with D_2O and an excess of the anesthetic molecule of interest (ethanol, diethyl ether and isoflurane). (b) Exemplary 2-dimensional data set (pure POPC bilayer), where pronounced Bragg-peaks become visible. (c) The 2-dimensional data were further reduced by integrating the data linearly along $q_{||}$ to create line scans. (Data vertically offset for clarity).

directly corresponds to an increased water concentration. The ethanol sample shows an increased experimental SLD mainly in the head group region; diethyl ether shows an increase in the bilayer center. From that we conclude that the experimentally observed additional water molecules are located within the membrane for both drugs. The strong impact of isoflurane on the SLD complicates an interpretation of these data. The apparent increased SLD in the bilayer can either be a result of incorporated isoflurane, the influx of water, or a combination of both effects. The SLD of isoflurane (see blue dashed line in Fig. 3(b)) is increased, however, rather flat in the bilayer center. On the other hand, the experimental SLD of the isoflurane sample shows a peak in the bilayer center (see Fig. 6(a)) and it can be speculated that this central increase indicates the location of the observed additional water molecules.

The umbrella-sampling simulations further support these claims. The potential mean force (PMF) $W(z)$ is narrowed in the presence of ethanol and significantly lowered in systems containing diethyl ether and isoflurane. Consequently, the partitioning of water within the membrane is drastically increased in the presence of these two potent anesthetics. Based on the results from our MD simulations, all drug molecules spontaneously partitioned in the bilayers within a few nanoseconds. Only when the drug molecules were present and equilibrated in the membranes, an increased number of water molecules was observed to enter the membranes as well. This is indicating that changes in membrane properties due to the presence of the drugs are more important than potential drug/water interactions.

While the experimental results and the water partitioning coefficient draw a static picture of increased intramembrane water in the presence of anesthetic molecules, many biological processes depend on transmembrane water transport, *i.e.*, the flux of water across the bilayer, as measured by the permeability P. Our results present evidence that the permeability of the bilayers is significantly increased in the presence of diethyl ether and isoflurane by factors of 1000 and 10 000, respectively (see Fig. 4). We note that the drug concentrations in this study were significantly above physiological relevance such that the observed effects are likely over-estimated.

It is still highly disputed if anesthetics work through specific interactions by binding to certain membrane receptors, or by acting on membrane proteins in a non-specific fashion through changing membrane properties. For the latter, it is also not clear what change in membrane property could induce an anesthetic function. In this work, we provide evidence that anesthetic molecules can significantly increase the amount of intramembrane water to be added to the list of membrane properties which are potentially affected by this drug family.

4 Conclusion

Anesthetic drugs are believed to interact non-specifically with cell membranes. However, despite numerous studies, a common mode of action of general anesthetic molecules remains unknown. While there seems to be a direct relation between the concentration of drug molecules in the membranes and their potency as anesthetics (the Meyer–Overton correlation), their impact on membrane properties and the connection to anesthetic function is not well understood. We investigated the impact of anesthetic molecules on the water content of a lipid membrane by combining MD simulations and neutron diffraction. Hydration water molecules were deuterium labeled in the experiments. The experiments provide direct evidence of an increased intramembrane water content in the presence of ethanol, diethyl ether and isoflurane molecules. This observation is confirmed by the MD simulations, which show a drastically (up

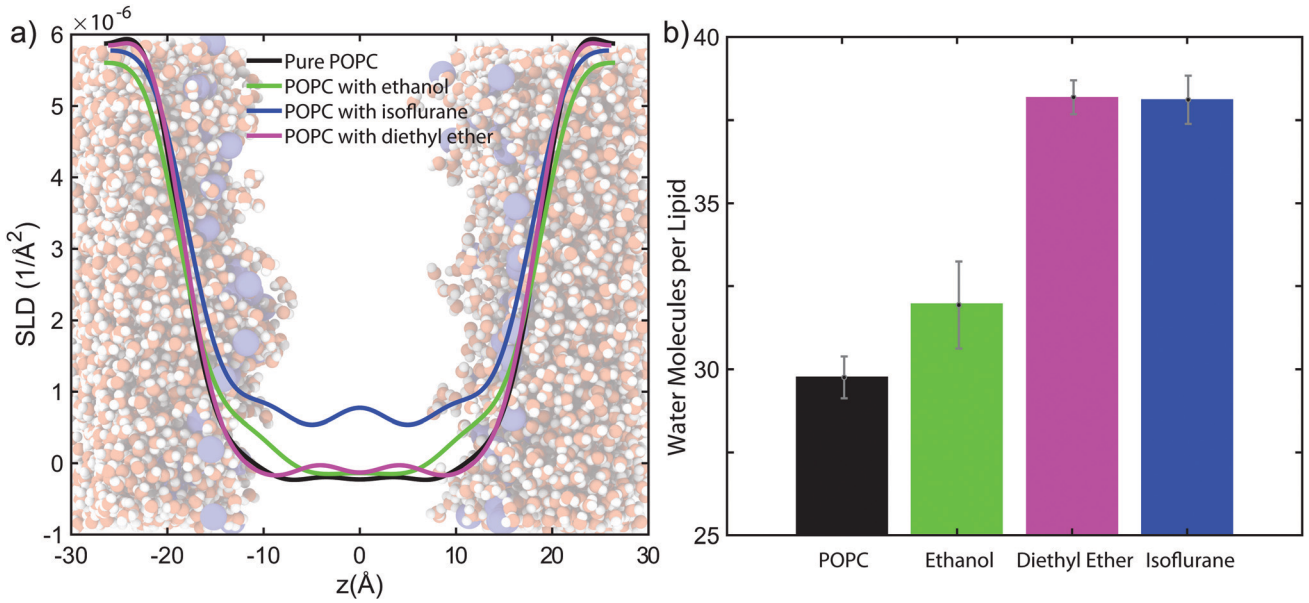

Fig. 6 (a) The experimentally determined scattering length density profile (SLD) resulting from a 1-dimensional Fourier analysis. The SLD is dominated by the contribution of D_2O on either side of the bilayer and is significantly reduced in the hydrophobic core. (b) The amount of water per lipid molecule can be determined by integrating the SLD profile and subtracting the contribution of POPC and the respective molecule.

to 60 fold) increased partitioning of water within the membrane and permeability (up to 10 000 fold). This significant increase in intramembrane water and its effect on membrane properties likely plays a role in the non-specific interactions of anesthetics with membranes.

5 Materials and methods

5.1 Molecular dynamics (MD) simulations

Molecular dynamic simulations were performed on MacSim, a GPU accelerated workstation. The computer is equipped with a 40 core central processing unit (CPU, Intel(R) Xeon(R) CPU E5-2630 v4), with 130 GB random access memory (RAM), as well as two Nvidia Geforce 1080Ti graphic processing units (GPU).

An all-atom membrane model consisting of 128 POPC molecules and 35 water molecules per lipid was created using the membrane generator on the charmm-gui website[20] and the Charmm 36 force-field.[21] All-atom models for dithylether, isoflurane, as well as ethanol were taken from the Automated Topology Builder and Repository (ATB) website[22] and the respective topology file was created using CHARMM General Force Field 4.0 (CgenFF).[23] All simulations were performed using GROMACS Version 5.1.2. First, the membrane system was allowed to equilibrate for 375 ps. Then, the membrane patch was allowed to simulate for additional 200 ns.

Membrane-Anesthetic complexes were created by first removing all water molecules from the equilibrated and simulated membrane. Then 200 molecules of the anesthetic were added using the built-in GROMACS tool. The system was then hydrated by adding 35 water molecules per lipid molecule, ensuring both an excess of water and anesthetic. All systems were equilibrated using a *NPT* ensemble. The simulations used a 2 fs time-step, a Van-der-Waal cutoff of 1.2 nm a Verlet cut-off scheme and periodic boundary conditions were applied in all three dimensions. The temperature was coupled using a Nose-hover thermostat (target temperature T = 303 K) and the pressure coupling was controlled using Parrinello–Rahman semi-isotropic weak coupling (τ = 5 ps; $\beta = 4.5 \times 10^{-5}$ bar^{-1}).

Neutron scattering length densities (SLDs) were determined from the simulated membrane patches using the GROMACS built-in density function. The commonly used *electron.dat* file was replaced by a file describing the corresponding neutron scattering length for each atom. Here, the scattering length of deuterium $\left(\mathrm{SL}\left({}^{2}_{1}\mathrm{H}\right) = 6.671\ \mathrm{fm}\right)$ was assigned to hydrogen atoms of water molecules while $\mathrm{SL}\left({}^{1}_{1}\mathrm{H}\right) = -3.7406$ fm was used for the remaining hydrogen atoms. The area per lipid was determined by dividing the area of the simulated lipid patch given by the lateral box dimension by the number of lipid molecules per leaflet (64).

Umbrella models were created out of the equilibrated and simulated membrane anesthetic patches by cropping a patch containing 72 Lipids while the lipid:water:anesthetic ratio was kept the same. Umbrella simulations were performed by isolating a single water molecule and fixing its z-position using a harmonic potential of 1064 kJ mol^{-1} (POPC, ethanol) 216 kJ mol^{-1} (isoflurane), 65 kJ mol^{-1} (diethyl ether). The molecule was then moved along the bilayer normal in steps of 1 Å and the patch was simulated for 20 ns. PMF profiles, $W(z)$, were then generated by using the GROMACS built-in weighted histogram analysis method (WHAM). These PMF profiles were then symmetrized between both leaflets.

As per design, umbrella sampling allows the direct calculation of the diffusivity profile $D(z)$ from the auto correlation function (ACF) utilizing the fluctuation dissipation theorem:[18,24]

$$D(z') = \frac{(RT)^2}{\int_0^\infty \langle \delta F(z,0)\delta F(z,t)\rangle} \mathrm{d}t, \quad (1)$$

where δF is the deviation of the lateral force on the solute molecule, R is the ideal gas constant and T is the Temperature. First, the ACF was computed for each position z of the confined water molecule using the GROMACS build-in analyze method. The integral in the denominator was then calculated using the trapezoidal method. The diffusivity profile was symmetrized between both leaflets.

The membrane permeability coefficient was evaluated using:[16,18]

$$\frac{1}{P} = \int_{-L/2}^{L/2} \frac{\mathrm{e}^{\beta W(z)}}{D(z)} \mathrm{d}z, \quad (2)$$

where L is the bilayer thickness.

The partitioning coefficient is defined as the ratio between the concentration of inserted water molecules C_m and the bulk water concentration C_w and can be expressed by:[16]

$$K = \frac{C_\mathrm{m}}{C_\mathrm{w}} = \frac{1}{L}\int_{-L/2}^{L/2} \mathrm{e}^{-\beta W(z)} \mathrm{d}z, \quad (3)$$

where $\beta = \frac{1}{RT}$.

5.2 Preparation solid supported membranes

20 mg of protonated 1-palmitoyl-2-oleoyl-*glycero*-3-phosphocholine (POPC) were dissolved in 1 ml of a 2,2,2-trifluoroethanol : chloroform (1 : 1,vol:vol) solution. Single-side polished silicon wafers (diameter: 100 mm; thickness: 0.53 mm) were cut in rectangles with a width of ~20 mm and a length of ~60 mm. The wafers where placed in 1,2-dichloromethane (DCM) and sonicated for 20 minutes at 40 °C leaving the surface in a hydrophobic state. The wafers were then rinsed with alternating methanol and ultra pure water (18.2 MΩ cm). The wafers were dried with inert nitrogen gas and placed on a hot (37 °C) plate. 1 ml of the POPC solution was applied and allowed to dry. The wafers were then placed in a vacuum chamber for 24 h and further incubated in an enclosed chamber for 48 h in a 98% relative humidity atmosphere created by a saturated K_2SO_4 solution.

5.3 Neutron diffraction experiment

In contrast to X-rays, neutrons interact with the atomic nuclei of atoms. While being indistinguishable for X-ray scattering, deuterium (^{2}H) has a ~3 times higher neutron scattering cross section as compared to hydrogen (^{1}H). By selectively labeling the membrane, anesthetic molecules and water molecules, the neutron diffraction experiment can be made sensitive specifically to the distribution of water molecules inside the bilayers.

All experiments were conducted on the D16 high-resolution neutron diffractometer on neutron guide H521 at the Institut Laue-Langevin (ILL) in Grenoble, France.[19] Data are available through the ILL using: https://doi.org/doi:10.5291/ILL-DATA.8-02-759. D16 was used in its 83° configuration at a neutron wavelength of λ = 4.55 Å. The experimental setup is schematically shown in Fig. 5(a). The sample was mounted inside a temperature and humidity controlled chamber (BerILL).[25] The chamber was operated at 37 °C and 97% relative humidity. The bassin of the chamber was filled with deuterium oxide (D_2O) together with 2 ml of the respective anesthetic molecule. All drugs were used in their protonated form and were purchased from Sigma Aldrich: ethanol (Cas: 64-17-5), diethyl ether (Cas: 60-29-7) isoflurane (Cas: 26675-46-7). Prior to each measurement, the sample was allowed to equilibrate for 120 minutes and the equilibrium was monitored by measuring the position of the first order diffraction peak. A measurement was started when the peak position stabilized and did not move within the experimental resolution.

Each measurement was performed in two steps: the 2-dimensional detector array was placed at 2θ = 12° and 2θ = 27° with respect to the incident beam tube. For each setting of the detector the sample is rotated between −1 and 8° and 8 and 18°, respectively. This results in a 2-dimensional neutron intensity map in reciprocal space covering a q-range between 0.06 and 0.87 Å^{-1}. The resulting 2-dimensional intensity map is further reduced by linear integration along the $q_{||}$ axis resulting in specular reflectivity scans.

The relative scattering length density (SLD), $\rho(z)$, is approximated by a 1-dimensional Fourier analysis:[26,27]

$$\rho(z) = \frac{2}{d_z}\sum_{n=1}^{N} \sqrt{I_n q_n}\nu_n \cos\left(\frac{2\pi n z}{d_z}\right). \quad (4)$$

N is the highest order of the Bragg peaks observed in the experiment. The integrated peak intensities, I_n, are multiplied by q_n to receive the form factors, $F(q_n)$.[26,27] The bilayer form factor $F(q_z)$, which is in general a complex quantity, is real-valued in the case of centro-symmetry. The phase problem of crystallography, therefore, simplifies to the sign problem $F(q_z) = \pm|F(q_z)|$ and the phases, ν_n, can only take the values ±1. The phases ν_n are needed to reconstruct the SLD-profile from the scattering data following eqn (4). When the membrane form factor $F(q_z)$ is measured at several q_z values, a continuous function, $T(q_z)$, which is proportional to $F(q_z)$, can be fitted to the data:[26,27]

$$T(q_z) = \sum_n \sqrt{I_n q_n}\, \mathrm{sinc}\left(\frac{1}{2}d_z q_z - \pi n\right). \quad (5)$$

Once an analytical expression for $T(q_z)$ has been determined from fitting the experimental peak intensities, the phases ν_n can be assessed from $T(q_z)$. The phase array $\nu_n = [-1\ 1\ -1\ -1\ 1\ -1]$ was used for all samples.

The SLD's determined by eqn (4) are on a relative scale. In contrast to the electron density known in X-ray crystallography, the scattering length density can have positive as well as negative values. The profiles were then scaled by first setting the minimum of each profile to 0. SLD profiles determined

from MD simulations (see above) were treated the same way. Each resulting graph was then integrated numerically using the trapezoidal method. The experimental SLD profile was then scaled by multiplying the unscaled profile $\rho^{\mathrm{exp}}_{\mathrm{unscaled}}$ with the fraction of the integrated simulated SLD I_{sim} to the integrated measured SLD I_{exp}:

$$\rho^{\mathrm{exp}}_{\mathrm{scaled}} = \frac{I_{\mathrm{exp}}}{I_{\mathrm{sim}}}\rho^{\mathrm{exp}}_{\mathrm{unscaled}}. \quad (6)$$

Finally the resulting graph was shifted such that the edge falls onto the simulated SLD of bulk water. The integrated scaled SLD multiplied with the area per lipid is equal to the total scattering length per unit cell. Thus the water content can be determined by subtracting the known scattering length of POPC and the anesthetic molecule, respectively, and dividing the result by the scattering length of D_2O (19.145 fm).[14] By design, the unit cell contains 2 lipid molecules (one per leaflet). The amount of water molecules per lipid is thus given by half the amount of water per unit cell.

Conflicts of interest

There are no conflicts to declare.

Acknowledgements

This research was funded by McMaster Universiy, the Natural Sciences and Engineering Research Council of Canada (NSERC), the Canada Foundation for Innovation (CFI) and the Ontario Ministry of Economic Development and Innovation. M. C. R. is the recipient of an Early Researcher Award of the Province of Ontario, and a McMaster University Scholar. The funders had no role in study design, data collection and analysis, decision to publish, or preparation of the manuscript. The authors thank the Institut Laue-Langevin in Grenoble, France, for the allocation of beam time and granting us access to laboratories within the Partnership for Soft Condensed Matter. All experimental data are available through the ILL using: https://doi.org/doi:10.5291/ILL-DATA.8-02-759.

Notes and references

1 R. Ashcroft, H. Coster and J. Smith, *Nature*, 1977, **269**, 819–820.
2 R. Westhorpe, *Anaesth., Pain Intensive Care*, 1996, **24**, 529.
3 H. Jerabek, G. Pabst, M. Rappolt and T. Stockner, *J. Am. Chem. Soc.*, 2010, **132**, 7990–7997.
4 N. P. Franks, *Br. J. Pharmacol.*, 2006, **147**, S72–S81.
5 H. Meyer, *Arch. Exp. Pathol. Pharmakol.*, 1899, **42**, 109–118.
6 H. Meyer, *Arch. Exp. Pathol. Pharmakol.*, 1901, **46**, 338–346.
7 C. E. Overton, *Studien über die Narkose: zugleich ein Beitrag zur allgemeinen Pharmakologie*, G. Fischer, 1901.
8 A. Missner and P. Pohl, *ChemPhysChem*, 2009, **10**, 1405–1414.
9 K. D. Hickey and M. M. Buhr, *J. Lipids*, 2011, **2011**, 208457.
10 N. Franks and W. Lieb, *J. Mol. Biol.*, 1979, **133**, 469–500.
11 D. Huster, A. J. Jin, K. Arnold and K. Gawrisch, *Biophys. J.*, 1997, **73**, 855–864.
12 G. Lahajnar, P. Macek, P. Smid and I. Zupancic, *Biochim. Biophys. Acta*, 1995, **1235**, 437–442.
13 L. Toppozini, C. L. Armstrong, M. A. Barrett, S. Zheng, L. Luo, H. Nanda, V. Garcia Sakai and M. Rheinstädter, *Soft Matter*, 2012, **8**, 11839–11849.
14 V. F. Sears, *J. Neutron Res.*, 1992, **3**, 26–37.
15 A. Volkov, S. Paula and D. Deamer, *Bioelectrochem. Bioenerg.*, 1997, **42**, 153–160.
16 A. Ghysels, A. Krämer, R. M. Venable, W. E. Teague, E. Lyman, K. Gawrisch and R. W. Pastor, *Nat. Commun.*, 2019, **10**, 1–12.
17 M. Darvas, P. N. Hoang, S. Picaud, M. Sega and P. Jedlovszky, *Phys. Chem. Chem. Phys.*, 2012, **14**, 12956–12969.
18 E. Awoonor-Williams and C. N. Rowley, *Biochim. Biophys. Acta, Biomembr.*, 2016, **1858**, 1672–1687.
19 V. Cristiglio, B. Giroud, L. Didier and B. Demé, *Neutron News*, 2015, **26**, 22–24.
20 S. Jo, T. Kim, V. G. Iyer and W. Im, *J. Comput. Chem.*, 2008, **29**, 1859–1865.
21 J. Huang, S. Rauscher, G. Nawrocki, T. Ran, M. Feig, B. L. de Groot, H. Grubmüller and A. D. MacKerell, *Nat. Methods*, 2017, **14**, 71–73.
22 A. K. Malde, L. Zuo, M. Breeze, M. Stroet, D. Poger, P. C. Nair, C. Oostenbrink and A. E. Mark, *J. Chem. Theory Comput.*, 2011, **7**, 4026–4037.
23 K. Vanommeslaeghe, E. Hatcher, C. Acharya, S. Kundu, S. Zhong, J. Shim, E. Darian, O. Guvench, P. Lopes and I. Vorobyov, *et al.*, *J. Comput. Chem.*, 2010, **31**, 671–690.
24 R. Kubo, *Rep. Prog. Phys.*, 1966, **29**, 255.
25 J. Gonthier, M. A. Barrett, O. Aguettaz, S. Baudoin, E. Bourgeat-Lami, B. Demé, N. Grimm, T. Hauß, K. Kiefer and E. Lelièvre-Berna, *et al.*, *J. Neutron Res.*, 2019, **21**, 65–76.
26 J. F. Nagle and M. C. Wiener, *Biophys. J.*, 1989, **55**, 309–313.
27 L. Toppozini, F. Roosen-Runge, R. I. Bewley, R. M. Dalgliesh, T. Perring, T. Seydel, H. R. Glyde, V. G. Sakai and M. C. Rheinstädter, *Soft Matter*, 2015, **11**, 8354–8371.

